calomel electrode (SCE) as the working, counter, and reference electrodes, respectively. Photocurrents as a function of electrode potential were measured with an EG & G 362 scanning potentiostat and recorded with an X-Y recorder (Houston Instruments, model RE0092). The intensity of the light source (in mW cm^{-2}) was measured by a radiometer (International Light Co., model IL 1350). The electrolyte, 5 M KOH, was freshly prepared using double-deionized water with resistivity of 18 megohms cm^{-1}. All solutions were prepared from analytical-grade reagents.

22. The photoconversion efficiency ε_{eff} (photo) of light energy to chemical energy in the presence of an external applied potential E_{app} can be expressed as

$$\% \ \varepsilon_{eff}(\text{photo}) = [j_p(E^0_{rev} - |E_{app}|)\times 100/(I_0)] \quad (1)$$

(*3*–*5*), where j_p is the photocurrent density, E^0_{rev} is the standard state-reversible potential (which is 1.23 V for the water-splitting reaction), I_0 is the intensity (power density) of the incident light, and $|E_{app}|$ is the absolute value of the applied potential E_{app}, which is obtained as

$$E_{app} = (E_{meas} - E_{aoc}) \quad (2)$$

(*3*–*5*), where E_{meas} is the electrode potential at which j_p was measured, and E_{aoc} is the electrode potential at open circuit in the same electrolyte solution and under the same illumination of light at which j_p was measured. For the CM-n-TiO_2 electrode, $E_{aoc} = -1.0$ volt/SCE was observed at illumination intensity of 40 mW cm^{-2} in 5 M KOH solution; E_{meas} and E_{doc} were with respect to the same reference electrode (SCE). Note that the total conversion efficiency of light and electrical energy to chemical energy, ε_{eff} (total), was calculated by neglecting E_{app} in Eq. 1.

23. R. E. Bird, R. L. Hulstrom, L. J. Leis, *Sol. Energy* **30**, 563 (1983).

13 June 2002; accepted 29 August 2002

The Origin of Aluminum Flocs in Polluted Streams

Gerhard Furrer,[1]* Brian L. Phillips,[2] Kai-Uwe Ulrich,[3] Rosemarie Pöthig,[4] William H. Casey[5]*

About 240,000 square kilometers of Earth's surface is disrupted by mining, which creates watersheds that are polluted by acidity, aluminum, and heavy metals. Mixing of acidic effluent from old mines and acidic soils into waters with a higher pH causes precipitation of amorphous aluminum oxyhydroxide flocs that move in streams as suspended solids and transport adsorbed contaminants. On the basis of samples from nine streams, we show that these flocs probably form from aggregation of the ε-Keggin polyoxocation $AlO_4Al_{12}(OH)_{24}(H_2O)_{12}^{7+}$(aq) ($Al_{13}$), because all of the flocs contain distinct $Al(O)_4$ centers similar to that of the Al_{13} nanocluster.

In studies of the aluminum geochemistry of acid mine drainage (*1*, *2*), solids were identified that precipitate at $4.2 < pH < 4.9$ as either x-ray–amorphous $Al(OH)_3$ or microcrystalline gibbsite. These flocs are fluffy (Fig. 1) and form as acidic effluent enriched in dissolved aluminum mixes with near-neutral surface water. A similar phenomenon occurs in watersheds where the load of acid rain critically exceeds the buffering capacity of the soil and parent rock (*3*). It is thought (*4*) that the flocs form by aggregation of monomeric aluminum complexes into a $Al_6(OH)_{12}(H_2O)_{12}^{6+}$ multimer that is structurally similar to dioctahedral sheets of gibbsite. Dissolved $Al_6(OH)_{12}(H_2O)_{12}^{6+}$, however, has never been detected, and this model has been challenged (*5*).

Here we propose an alternative explanation. We examined flocs from nine polluted streams in Germany and California (Table 1) (table S1 and figs. S2 to S4) with ^{27}Al magic-angle spinning (MAS) nuclear magnetic resonance (NMR) spectroscopy, which resolves aluminum atoms with different coordination environments. The ^{27}Al NMR spectra of all field samples exhibit signals near +63 and +35 parts per million (ppm), which indicate the presence of substantial amounts of aluminum in tetrahedral form [$Al(O)_4$] and in coordination to five oxygen atoms [$Al(O)_5$] (*6*), in addition to the dominating $Al(O)_6$ peak near +7 ppm. Because the spectra of all samples were similar, we selected three samples to show the range in relative intensities (Fig. 2A). The first and last samples (Fig. 2A, top and bottom) have the most and least amounts of $Al(O)_4$, respectively. The sec-

Fig. 1. Aluminum oxyhydroxide floc on a streambed in Yuba County, California. The white aluminum oxyhydroxide floc overlies orange iron oxyhydroxide solids. Image width, ≈30 cm.

[1]Institute of Terrestrial Ecology, Eidgenössische Technische Hochschule Zürich, Grabenstrasse 3, CH-8952 Schlieren, Switzerland. [2]Department of Geosciences, State University of New York, Stony Brook, NY 11794–2100, USA. [3]Technical University of Dresden, Ecological Station Neunzehnhain, D-09514 Lengefeld, Germany. [4]Leibniz Institute of Freshwater Ecology and Inland Fisheries, Müggelseedamm 310, D-12587 Berlin, Germany. [5]Department of Land, Air, and Water Resources and Department of Geology, University of California, Davis, CA 95616, USA.

*To whom correspondence should be addressed. E-mail: furrer@ito.umnw.ethz.ch (G.F.); whcasey@ucdavis.edu (W.H.C.)

Table 1. Characterization of the selected field samples of representative aluminum oxyhydroxide flocs, collected from 1996 to 2001. Some samples were centrifuged immediately after collection and then dried under ambient conditions. Other samples (e.g., those from Spenceville) were analyzed both as a wet paste and as an air-dried gel. The aluminum concentrations were measured in the 0.45 μm–filtered water samples from the mixing zones. For the sample shown in Fig. 2A, middle, values are not available from direct in situ measurements in the mixing zone because the acid mine effluent (pH = 2.3; 1 mM < ΣAl < 15 mM) enters the pristine stream water [pH = 7.7; ΣAl < detection limit (d.l.)] from the hyporheic zone.

Sample spectrum	Geographic region	Geology	Vegetation	Type of pollution	Sampling date	pH in mixing zone	Aluminum concentration
Fig. 2A, top	East Thuringian, Slate Mountains, Germany	Carboniferous blue slate	Mixed forest	Acid mine drainage	22 May 1998	5.0 to 6.5	20 to 180 μM
Fig. 2A, middle	Spenceville, Yuba County, California	Metavolcanic rocks	Mixed forest	Acid mine drainage	4 Jan 2001	—	0 to 16 mM
Fig. 2A, bottom	Ore Mountains, Saxony, Germany	Mica slate, gneisses	Spruce	Acid rain	25 Mar 1999	5.0 to 5.5	18 to 60 μM

ond sample (Fig. 2A, middle) is typical of the seven other samples. The concentration of $Al(O)_4$ reached ≈7% of the total Al(III) (Fig. 2A, top). The signal near +63 ppm cannot be attributed to clay, such as illite or smectite, which would yield a peak near +70 ppm (*7*). Examination of the field samples by x-ray diffraction did not show any crystalline phase other than traces of quartz. Similar ^{27}Al NMR spectra have been reported from flocs in organic-rich lake waters that are also rich in aluminum (*8*).

The stable $Al(OH)_3$ minerals (gibbsite, bayerite) contain only sheets of edge-linked $Al(O)_6$, leading us to the hypothesis that the high $Al(O)_4$ concentrations in the stream flocs are structural remnants of dissolved aluminum molecules. There are only three species in acidic aqueous solutions that have $A1(O)_4$: the mononuclear $Al(OH)_4^-$(aq) and the polyoxocations $AlO_4Al_{12}(OH)_{24}(H_2O)_{12}^{7+}$(aq) ($Al_{13}$), which has an ε-Keggin–like structure (Fig. 3), and $(AlO_4)_2Al_{28}(OH)_{56}(H_2O)_{24}^{18+}$(aq) ($Al_{30}$), the structure of which has recently been resolved (*9*, *10*). This molecule can be synthesized within hours only at elevated temperature (95°C), so it is unlikely to form in streams.

Under equilibrium conditions, the Al_{13} polyoxocation can account for much more of the total $Al(O)_4$ in the polluted waters than the monomeric $Al(OH)_4^-$(aq) complex. With accepted equilibrium constants (*11*, *12*), Al_{13} is predicted to form at total dissolved aluminum concentrations (ΣAl) of more than 20 μM at pH > 5. The filtered waters from our field sites (Table 1) exhibit 20 μM < ΣAl < 180 μM and 5.0 < pH < 5.5. At metastable equilibrium, a solution with pH = 5.0 and ΣAl = 100 μM contains 78% of ΣAl in the form of Al_{13}, whereas $Al(OH)_4^-$(aq) makes up only 0.01%. The other 22% are distributed almost equally between the monomeric species Al^{3+}(aq), $Al(OH)^{2+}$(aq), and $Al(OH)_2^+$(aq). In such a solution, $Al(O)_4$ amounts to at least 6% of ΣAl, and the amount of $Al(O)_4$ incorporated in Al_{13} is 600 times that in $Al(OH)_4^-$(aq). Although equilibrium calculations give no information about disequilibrium pathways, they indicate that Al_{13} is potentially abundant and that virtually all aluminum-rich acid drainage waters pass through the Al_{13} metastability field during mixing with pristine surface waters. Because Al_{13} forms quickly in aqueous solution, disequilibrium caused by poor mixing of the acidic and basic solutions will result in even greater concentrations of Al_{13} than indicated by the calculations.

Because the Al_{13} molecule is sufficiently unreactive once formed, it can retain vestigial $Al(O)_4$ if polymerized rapidly into a solid as the pH rises and causes bound water ligands to deprotonate. At conditions typical for polluted streams, decomposition of Al_{13} molecules takes hundreds of hours (e.g., half-life ≈ 580 hours at pH = 5 and 283 K) (*13*), as does the exchange of structural oxygens with bulk solution (*14*); yet it is evident that Al_{13} forms within minutes, which is the minimum time necessary to collect an ^{27}Al NMR spectrum.

We synthesized flocs with aluminum solutions under conditions similar to those encountered during mixing of acidic mine waters with neutral surface waters. In all cases, the resulting gels contained substantial amounts of $Al(O)_4$ and $Al(O)_5$, even when the titrations were conducted rapidly and at low temperature (Fig. 2B, bottom). The supernatant solution usually contained detectable Al_{13}, which is evident in spectra of wet gels.

We repeated the experiments with solutions that do not contain $Al(OH)_4^-$(aq) to determine whether Al_{13} can account for $Al(O)_4$ observed in the field samples. We performed experiments with monospecific Al_{13} solutions and with monospecific $GaO_4Al_{12}(OH)_{24}(H_2O)_{12}^{7+}$(aq) ($GaAl_{12}$) solutions. This $GaAl_{12}$ molecule has gallium substituted exclusively into the central tetrahedral site (*15*) and no $Al(O)_4$. As expected, if Al_{13} was the source of $Al(O)_4$ in the gel, we observed retention of $Al(O)_4$ when Al_{13} molecules were condensed in solution, but we did not observe $Al(O)_4$ when $GaAl_{12}$ was aggregated.

This experiment shows that the coordination of the tetrahedral center is retained in the solid when the molecules are condensed into a gel. Accordingly, the ^{71}Ga MAS NMR spectrum (9.4 T) of the same gel gave a relatively broad peak for tetrahedrally coordinated gallium centered near 122 ppm (*15*). However, the gels obtained from monospecific Al_{13} solutions do not contain a distinct signal for $Al(O)_5$, which suggests that these sites form by interaction of Al_{13} with monomeric aluminum complexes, which were excluded from the solutions.

Because Al_{13} formation is suppressed in the presence of high sulfate concentrations (*16*), we also conducted several experiments simulating the slow dilution of acid mine water, containing 0.1 M $AlCl_3$ and 0 to 0.6 M sulfate, into water

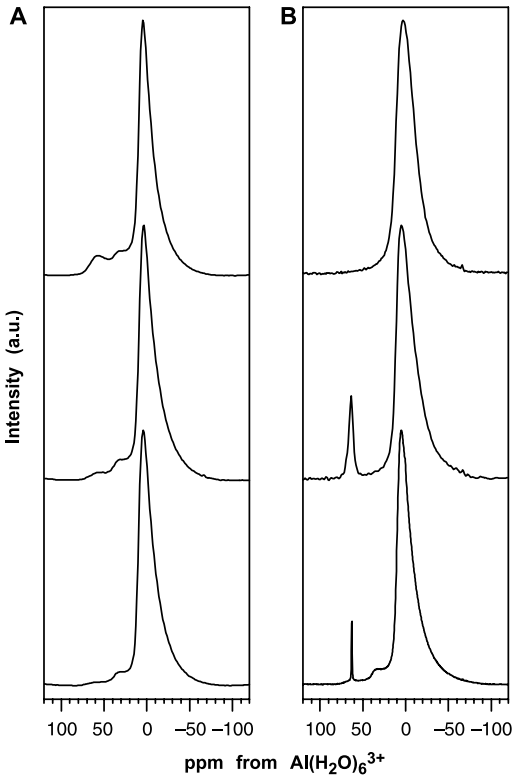

Fig. 2. Selection of ^{27}Al MAS NMR spectra (*28*) of natural and synthetic aluminum oxyhydroxide gels. The prominent broad peaks near 0 ppm indicate $Al(O)_6$ environments. The signals near +60 and +35 ppm correspond to $Al(O)_4$ and $Al(O)_5$, respectively. The fractions of four- and five-coordinated aluminum are 1 to 7% for $Al(O)_4$ and 5 to 9% for $Al(O)_5$. The nature of $Al(O)_5$ is uncertain, but it may originate from $Al(O)_6$ because some samples exhibit total intensities for $Al(O)_4$ and $Al(O)_5$ that exceed $\frac{1}{13}$, the stoichiometric $Al(O)_4$ fraction for Al_{13}. (**A**) Spectra of representative aluminum oxyhydroxide flocs from streams polluted by acid mine drainage in Germany (top) and in California (middle) and from the junction of a stream acidified by acid rain and a neutral stream in Germany (*3*) (bottom). The intensity of the $Al(O)_4$ signal in the top spectrum corresponds to 7(±1)% of the total aluminum. (**B**) Spectra of synthetic flocs. No signals for $Al(O)_4$ or $Al(O)_5$ are observed if the gels are made from $GaAl_{12}$ molecules (*29*) (top). A peak near +60 ppm is seen in the spectra of a gel that is made by neutralizing an acidic aqueous solution containing dissolved Al_{13} as the only aluminum species (*29*) (middle). In addition to peaks for $Al(O)_4$ and $Al(O)_5$ in the solid phase, a sharp peak for Al_{13} in the fluid (bottom) was found in a gel that was generated at ~5°C by instantaneous mixing of 0.2 M $AlCl_3$ and 0.48 M NaOH at equal volumes and analyzed within 30 min.

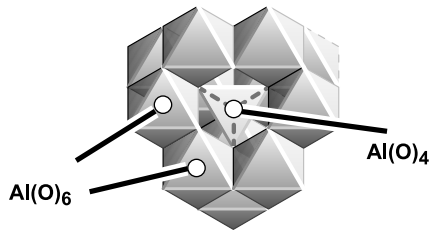

Fig. 3. The structure of the Al_{13} nanocluster in polyhedral presentation. The complex with the stoichiometry $AlO_4Al_{12}(OH)_{24}(H_2O)_{12}^{7+}$(aq) is composed of a central $Al(O)_4$ surrounded by 12 equivalent octahedrally coordinated aluminum atoms. Above pH ≈ 5.5, the charge of the polymer is lost by partial deprotonation of the 12 terminal water molecules (*26*). This triggers condensation of the nanoclusters into an x-ray–amorphous gel that eventually forms bayerite (*27*).

buffered by marble chips. At all $\Sigma SO_4/\Sigma Al(III)$ ratios, we found substantial amounts of $Al(O)_4$ and $Al(O)_5$ in the flocs after separation from the marble chips.

A close genetic link between Al_{13} and solid aluminum hydroxides has been postulated (*17*, *18*). However, the Al_{13} species is difficult to observe in nature because the pH window between formation and aggregation is small and because mixing of polluted and unpolluted waters is usually rapid and episodic. All of our results support the hypothesis that the aluminum flocs commonly found in polluted streams originate mainly from condensation of Al_{13} molecules that form rapidly and then aggregate as pH of the effluent increases to more than 5.

These results are important because Al_{13} is phytotoxic (*5*, *19*) and is probably responsible for the decline of fish populations in rivers polluted by mine drainage and acid rain (*20*). Its longevity and chemical affinity for heavy-metal cations, such as Pb^{2+}, Cu^{2+}, or Zn^{2+} (table S1) (*21*), suggest that dissolved Al_{13} and suspended aluminum flocs can transport metals downstream over considerable distances.

References and Notes

1. D. K. Nordstrom, *Geochim. Cosmochim. Acta* **46**, 681 (1982).
2. _____, J. W. Ball, *Science* **232**, 54 (1986).
3. K.-U. Ulrich, R. Pöthig, *Acta Hydrochim. Hydrobiol.* **28**, 313 (2000).
4. R. W. Smith, J. D. Hem, *U.S. Geol. Surv. Water Supply Pap. 1827-D* (1972).
5. P. M. Bertsch, D. R. Parker, in *The Environmental Chemistry of Aluminum*, G. Sposito, Ed. (CRC Press, Boca Raton, FL, ed. 2, 1996), pp. 117–168.
6. Peak positions correspond to the data taken at 16.4 T, which are less affected by second-order quadrupolar shifts. Peak positions at 9.4 T are 3 to 5 ppm more negative than those at 16.4 T. Assignment of the peak near +35 ppm to $Al(O)_5$ is based on the similarity of this chemical shift to those observed for crystalline phases that contain aluminum in coordination to five oxygens (*22–25*).
7. D. E. Woessner, *Am. Mineral.* **74**, 203 (1989).
8. A. Masion *et al.*, *Environ. Sci. Technol.* **34**, 3242 (2000).
9. L. Allouche, C. Gérardin, T. Loiseau, G. Férey, F. Taulelle, *Angew. Chem. Int. Ed.* **39**, 511 (2000).
10. J. Rowsell, L. F. Nazar, *J. Am. Chem. Soc.* **122**, 3777 (2000).
11. D. K. Nordstrom, H. M. May, in *The Environmental Chemistry of Aluminum*, G. Sposito, Ed. (CRC Press, Boca Raton, FL, ed. 2, 1996), pp. 39–80.
12. G. Furrer, B. Trusch, C. Müller, *Geochim. Cosmochim. Acta* **56**, 3831 (1992).
13. G. Furrer, M. Gfeller, B. Wehrli, *Geochim. Cosmochim. Acta* **63**, 3069 (1999).
14. B. L. Phillips, W. H. Casey, M. Karlsson, *Nature* **404**, 379 (2000).
15. S. M. Bradley, R. A. Kydd, C. A. Fyfe, *Inorg. Chem.* **31**, 1181 (1992).
16. J.-P. Boisvert, C. Jolicoeur, *Colloids Surf. A: Physicochem. Eng. Aspects* **155**, 161 (1999).
17. J. Y. Bottero *et al.*, *J. Colloid Interface Sci.* **117**, 47 (1986).
18. D. Hunter, D. S. Ross, *Science* **251**, 1056 (1991).
19. D. R. Parker, T. B. Kinraide, L. W. Zelazny, *Soil Sci. Soc. Am. J.* **53**, 789 (1989).
20. A. B. S. Poleo, *Aquat. Toxicol.* **31**, 347 (1995).
21. B. Lothenbach, G. Furrer, R. Schulin, *Environ. Sci. Technol.* **31**, 1452 (1997).
22. M. C. Cruikshank *et al.*, *J. Chem. Soc. Chem. Comm.* **1986**, 23 (1986).
23. L. B. Alemany, G. W. Kirker, *J. Am. Chem. Soc.* **108**, 6158 (1986).
24. B. L. Phillips, F. M. Allen, R. J. Kirkpatrick, *Am. Mineral.* **72**, 1190 (1987).
25. D. Massiott *et al.*, *Magn. Reson. Chem.* **28**, S82 (1990).
26. G. Furrer, Chr. Ludwig, P. W. Schindler, *J. Colloid Interface Sci.* **149**, 56 (1992).
27. S. M. Bradley, R. A. Kydd, R. F Howe, *J. Colloid Interface Sci.* **159**, 405 (1993).

28. The ^{27}Al MAS NMR spectra were recorded in spring 2001 on a Chemagnetics CMX spectrometer at 104.25 MHz with single-pulse excitation, a pulse width of 1 μs, a relaxation delay of 0.1 s, and a digitizing rate of 500 kHz. The samples were placed in sealed rotors (4-mm outside diameter) and spun at 15 to 16 kHz. The spinning sidebands lie outside of the displayed spectral range. Synthetic gel samples were examined wet, immediately after centrifugation, and after drying under ambient conditions, but no substantial difference was noted in the ^{27}Al MAS NMR spectra. Additional spectra were taken several months later at 182.4 MHz with a Bruker Avance spectrometer and similar acquisition conditions, except that the spinning rate was 30 kHz. These spectra are much better resolved and confirmed the estimates of relative populations of coordination environments.

29. The solutions were prepared by metathetic dissolution of the corresponding Al_{13}- or $GaAl_{12}$-selenate crystals in the presence of dissolved $BaCl_2$ (*14*, *15*, *26*, *27*).

30. Financial support came from the NSF, the U.S. Department of Energy, and Eidgenössische Technische Hochschule Zürich. Much of the work was conducted at University of California, Davis, during G.F.'s sabbatical leave. We thank A. P. Lee, P. Yu, and M. Ziliox for technical assistance; B. Wehrli and A. C. Johnson for valuable discussions; and R. Schulin and L. Paul for general support. Inductively coupled plasma–mass spectrometry analyses were provided by A. Birkefeld.

Supporting Online Material

www.sciencemag.org/cgi/content/full/297/5590/2245/DC1

Figs. S2 to S4

Table S1

8 July 2002; accepted 16 August 2002

Hydrogen Clusters in Clathrate Hydrate

Wendy L. Mao,[1,2]* Ho-kwang Mao,[2] Alexander F. Goncharov,[2] Viktor V. Struzhkin,[2] Quanzhong Guo,[2] Jingzhu Hu,[2] Jinfu Shu,[2] Russell J. Hemley,[2] Maddury Somayazulu,[3] Yusheng Zhao[4]

High-pressure Raman, infrared, x-ray, and neutron studies show that H_2 and H_2O mixtures crystallize into the sII clathrate structure with an approximate H_2/H_2O molar ratio of 1:2. The clathrate cages are multiply occupied, with a cluster of two H_2 molecules in the small cage and four in the large cage. Substantial softening and splitting of hydrogen vibrons indicate increased intermolecular interactions. The quenched clathrate is stable up to 145 kelvin at ambient pressure. Retention of hydrogen at such high temperatures could help its condensation in planetary nebulae and may play a key role in the evolution of icy bodies.

Hydrogen-bonded H_2O frameworks form a remarkable number of pure ice phases (*1–3*) and can build polyhedron cages around guest molecules to form solid clathrate hydrates, thus trapping the guest molecules at temperatures and pressures at which they would otherwise exist as free gases (*4–9*). With each cage singly occupied by a guest molecule, clathrates at ambient pressure are limited to a guest/H_2O molecular ratio $R \sim 1/6$ (Villard's rule). Recently, multiple occupancy of the large cage in sII clathrate by small molecules has been recognized in high-pressure experiments (*10–12*) and theoretical simulations (*13, 14*). Dyadin *et al.* (*12*) suggested the possibility of R as high as 1/3. Hydrogen and water are by far the most abundant gas and ice components in the solar system, but with a diameter of 2.72 Å, hydrogen molecules were thought to be too small to support a clathrate structure. Instead, hydrogen molecules were found to fill small cavities in ice II and ice Ic (*15*) at high pressures.

Here we report the synthesis of a hydrogen hydrate with the classical sII structure (HH-sII) with $R = 0.45 \pm 0.05$ (*16*). This requires that the small cages be doubly occupied and the large cages be quadruply occupied by clusters of hydrogen molecules. HH-sII is stable (or metastable) to ambient pressure and low temperature after initial synthesis at a moderate pressure. In a diamond anvil cell (DAC), we compressed a mixture of H_2 and H_2O to pressures of 180 to 220 MPa at 300 K. The samples were clearly separated into two regions: a H_2 bubble and liquid water. Upon cooling to 249 K, the two fluids were observed to react and form a single, solid compound. These phases were monitored in situ using a variety of probes. Using energy-dispersive x-ray diffraction (EDXD) at the X17B beamline of the National Synchrotron Light Source (NSLS), we observed 21 diffraction peaks at 220 ± 30 MPa and 234 K (table S1). The EDXD pattern in

[1]Department of the Geophysical Sciences, University of Chicago, Chicago, IL 60637, USA. [2]Geophysical Laboratory, Carnegie Institution of Washington, Washington, DC 20015, USA. [3]High Pressure Collaborative Access Team, Advanced Photon Source, Argonne National Laboratory, Argonne, IL 60439, USA. [4]Los Alamos Neutron Science Center (LANSCE), Los Alamos National Laboratory, Los Alamos, NM 87545, USA.

*To whom correspondence should be addressed. E-mail: wmao@uchicago.edu